Since January 2020 Elsevier has created a COVID-19 resource centre with free information in English and Mandarin on the novel coronavirus COVID-19. The COVID-19 resource centre is hosted on Elsevier Connect, the company's public news and information website.

Biosensors and Bioelectronics 229 (2023) 115221

Contents lists available at ScienceDirect

Biosensors and Bioelectronics

journal homepage: www.elsevier.com/locate/bios

Sensitive SARS-CoV-2 salivary antibody assays for clinical saline gargle samples using smartphone-based competitive particle immunoassay platforms

Yan Liang [a,1], Bailey C. Buchanan [b,1], Bradley Khanthaphixay [b], Avory Zhou [b], Grace Quirk [c], Michael Worobey [c], Jeong-Yeol Yoon [a,b,*]

[a] Department of Chemistry and Biochemistry, The University of Arizona, Tucson, AZ, 85721, United States
[b] Department of Biomedical Engineering, The University of Arizona, Tucson, AZ, 85721, United States
[c] Department of Ecology and Evolutionary Biology, The University of Arizona, Tucson, AZ, 85721, United States

ARTICLE INFO

Keywords:
COVID-19
Capillary action
Smartphone-based fluorescence microscope
Receptor-binding domain
Saline gargle
Omicron variant

ABSTRACT

Antibody assay for SARS-CoV-2 has become increasingly important to track latent and asymptomatic infections, check the individual's immune status, and confirm vaccine efficacy and durability. However, current SARS-CoV-2 antibody assays require invasive blood collection, requiring a remote laboratory and a trained phlebotomist. Direct detection of SARS-CoV-2 antibodies from clinical saline gargle samples has been considered challenging due to the smaller number of antibodies in such specimens and the high limit of detection of currently available rapid tests. This work demonstrates simple and non-invasive methods for detecting SARS-CoV-2 salivary antibodies. Competitive particle immunoassays were developed on a paper microfluidic chip using the receptor-binding domain (RBD) antigens on spike proteins. Using a smartphone, they were monitored by counting the captured fluorescent particles or evaluating the capillary flow velocities. The limit of detection (LOD), cross-binding between alpha- and omicron-strains, and the effect of angiotensin-converting enzyme 2 (ACE2) presence were investigated. LODs were 1–5 ng/mL in both 10% and 1% saliva. Clinical saline gargle samples were assayed using both methods, showing a statistical difference between virus-negative and virus-positive samples, although the assays targeted antibodies. Only a small number of virus-positive samples were antibody-negative. The high assay sensitivity detected a small number of antibodies developed even during the early phase of infections. Overall, this work demonstrates the ability to detect SARS-CoV-2 salivary IgG antibodies on simple, cost-effective, portable platforms towards mitigating SARS-CoV-2 and potentially other respiratory viruses.

1. Introduction

The coronavirus-19 (COVID-19) pandemic has significantly impacted the world. This disease is caused by severe acute respiratory syndrome coronavirus (SARS-CoV-2) that can spread quickly (Rai et al., 2021). Various COVID-19 vaccines have been developed since 2020 to prevent or alleviate infection-related morbidity (Wu et al., 2022). COVID-19 vaccines cause the immune system to create antibodies against the SARS-CoV-2 virus, and the harmless version of the virus' spike protein was used for vaccines. The human body's immunoglobulin G (IgG) and immunoglobulin M (IgM) levels were usually elevated after vaccination. This elevation is similar to the antibody responses in infected patients (Hartanto et al., 2020). The immune seroconversion reaches its maximum typically after 5–7 days of symptom onset for IgG and several days later for IgM (Long et al., 2020). Studies have shown the close relationship between antibody amount and virus neutralization, proposing a potent correlation with immune protection (Khoury et al., 2021; To et al., 2020). Instead of antigen detection, antibody assays could provide more information about an individual's immune status, tracking infection symptoms, confirming vaccination protection, and checking vaccine durability (Wu et al., 2022). Moreover, the United States National Institutes of Health (NIH) has uncovered millions of hidden, uncounted COVID-19 cases through antibody studies (Kalish et al., 2021).

* Corresponding author. Department of Chemistry and Biochemistry, The University of Arizona, Tucson, AZ, 85721, United States.
E-mail address: jyyoon@arizona.edu (J.-Y. Yoon).
[1] These authors contributed equally.

https://doi.org/10.1016/j.bios.2023.115221
Received 16 December 2022; Received in revised form 23 February 2023; Accepted 8 March 2023
Available online 12 March 2023

There has not been an extensive demonstration of portable SARS-CoV-2 antibody detection (Kopel et al., 2021). Some lateral flow assays have been developed to detect SARS-CoV-2 IgM or IgG antibodies. However, all of these assays require a blood sample. Therefore, a licensed phlebotomist should collect sufficient blood through an invasive procedure (Norman et al., 2020; Tollånes et al., 2020; Yakoh et al., 2021; Younes et al., 2020). There is a need to develop a handheld, low-cost antibody assay from saliva samples. A saliva sample offers a non-invasive collection method and adds to the ease of the assay. However, the number of antibodies available in saliva samples is lower than in blood samples, especially considering that the saliva samples are diluted through gargling (Breshears et al., 2022). The limit of detection (LOD) of commercial SARS-CoV-2 rapid antigen tests (with swabs in Amies) ranged from 5000 to 500,000 pfu/mL $= 0.8 \times 10^7 - 5.4 \times 10^8$ genome copies/mL. Considering the mass of a single SARS-CoV-2 virus of around 1 fg, these LODs corresponded to 12–540 ng/mL (Cubas-Atienzar et al., 2021), which may not be sufficient to detect antibodies from saline gargle samples, especially during the initial phases of infection or vaccination.

Here we present a work for salivary antibody detection using a smartphone through a microfluidic competitive immunoassay. Previously, we detected SARS-CoV-2 antigens using particle immunoagglutination on paper microfluidic chips (Akarapipad et al., 2022; Breshears et al., 2022). Both antibody-conjugated polystyrene particles and target antigens were free to flow through paper pores. Antibody-antigen binding made the particles aggregate (immunoagglutination), which could be quantified by smartphone-based fluorescence microscopic imaging (Breshears et al., 2022) or the changes in capillary flow velocity (arising from the changes in interfacial tension) (Akarapipad et al., 2022). These two methods have successfully demonstrated low LODs from saline gargle samples. For antibody assay, antigens should be conjugated to the particles. Since the SARS-CoV-2 antigens are much smaller than antibodies, particle immunoagglutination rarely occurs, requiring a different assay format. Therefore, we implemented a competitive particle immunoassay, as depicted in Fig. 1c. Antibodies were pre-loaded to the test zone of the microfluidic channel and paper fibers could immobilize antibodies by supramolecular interactions (Ratajczak et al., 2022; Ratajczak and Stobiecka, 2022). With no target presence, antigen-conjugated particles are captured in the antibody pre-loaded area, which can be imaged and detected by a smartphone-based fluorescence microscope (Fig. 1c). Many particles are captured, leaving a small number of particles in the moving front, resulting in a minimum decrease in interfacial tension and capillary flow velocity. The capillary flow velocity is proportional to the interfacial tension according to the Lucas-Washburn equation (Klug et al., 2018). The particle concentration is too low to affect the overall liquid viscosity, as demonstrated by our previous work (Klug et al., 2018). Therefore, the number of particles at the moving front determines the interfacial tension and contact angle, ultimately affecting the flow velocity (Fig. 1c). With target antibody presence, antigen-conjugated particles prefer to bind to the free-moving antibodies in the sample, leaving a minimum number of particles in the antibody pre-loaded area. Many antibody-bound particles can be found at the moving front, resulting in a substantial decrease in interfacial tension and capillary flow velocity. For both methods, signals should decrease with increasing antibody concentration.

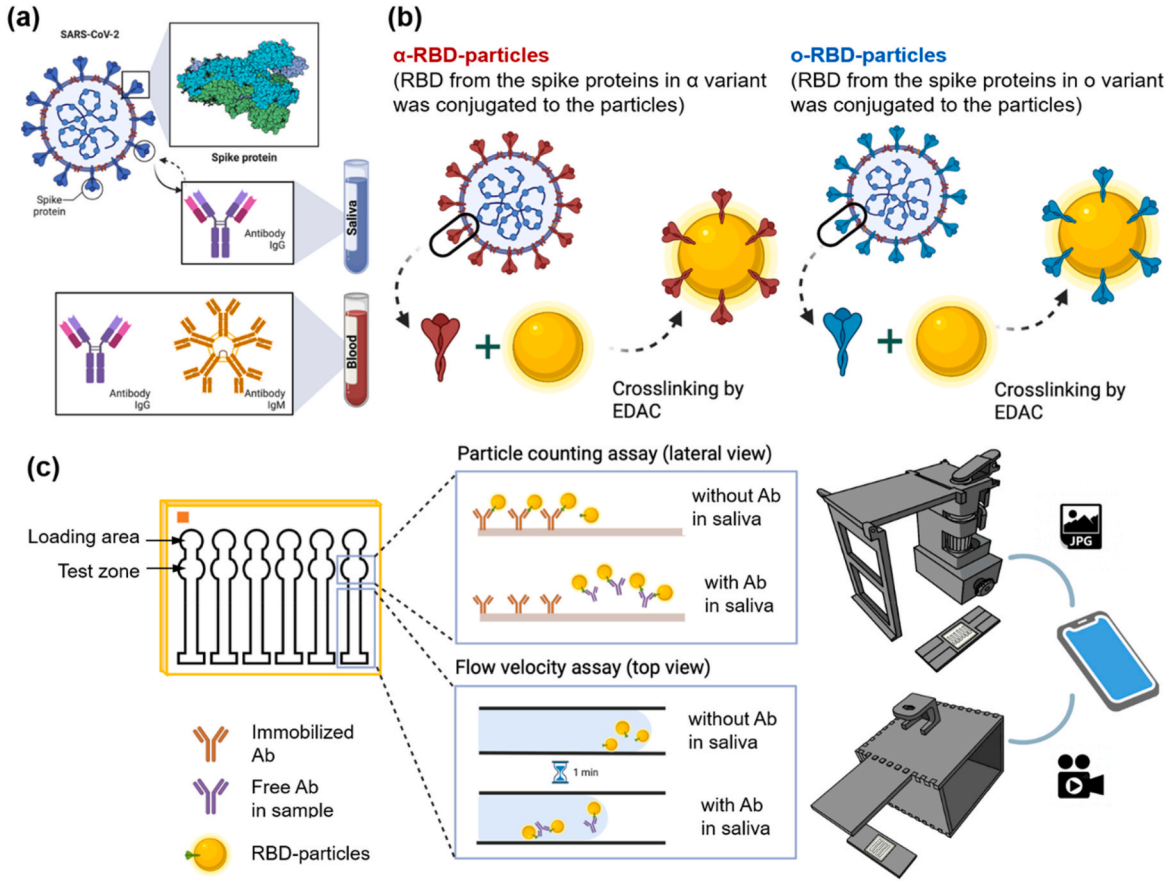

Fig. 1. Assay principle. (a) SARS-CoV-2 spike proteins and the antibody presence (IgG and IgM) in saliva and blood. (b) Two different RBD antigens from the spike proteins in α and o variants were covalently conjugated to the fluorescent polystyrene particles using 1-ethyl-3-(3-dimethylaminopropyl)carbodiimide (EDAC) chemistry. (c) Schematics of particle counting and flow velocity measurements using a smartphone-based fluorescence microscope and the smartphone-based video capture.

The receptor-binding domain (RBD) on the spike protein functions to bind to human cellular receptors, triggering cascaded events of membrane fusions for cell entry (Fig. 1a) (Norman et al., 2020; Heinz and Stiasny, 2021; Huang et al., 2020). RBD binds to the cell receptor human angiotensin-converting enzyme 2 (ACE2), acting as a critical factor in cell entry and virus spreading (Huang et al., 2020; Long et al., 2020; Windsor et al., 2022). Additionally, RBD is an essential target for neutralizing antibodies (e.g., anti-RBD) that are generated after infection or vaccination (Wu et al., 2022). We crosslinked the virus RBD antigens from the alpha (α) or omicron (ο) strains to the fluorescent particles to form a virus-structure-similar indicator for antibody detection (Fig. 1b). Anti-RBD-IgG was initially chosen as a target due to its relative dominance in human saliva and earlier dynamic changes after virus infection or vaccination (Alkharaan et al., 2021). Moreover, anti-RBD-IgG is related to virus neutralization and immune protection after infection or vaccination (Heinz and Stiasny, 2021; Huang et al., 2020). Clinical samples gathered during the SARS-CoV-2 outbreaks of α variant were tested on our platforms when vaccines were unavailable, and thus the antibodies in clinical samples were exclusively made from infection.

This work also aimed to compare the working conditions and advantages of two detection methods. Both methods were applied to the same chips to compare them appropriately: 1) antibodies were pre-loaded and dried, 2) antigen-conjugated particles were loaded and dried, 3) samples were loaded, 4) the capillary flow velocities were measured, and 5) the smartphone-based fluorescence microscopic images were captured after all samples were dried. Steps 1) and 2) can be prepared prior to the assays in practical applications. The flow velocities were measured from a video captured through a smartphone camera. A Python script was used to analyze the videos through Google Colaboratory. The average pixel areas of the particles captured in the antibody pre-loaded area (test zone) were evaluated using a smartphone camera with a microscope attachment, a light emitting diode (LED), and an acrylic color filter film. Images were processed through an ImageJ batch macro code. Each method offered unique advantages and working conditions that would be further discussed.

There is a limited amount of research on detecting SARS-CoV-2 antibodies, and current methods for antibody detection rely almost solely on blood samples, requiring invasive sampling. We demonstrate the ability of non-invasive, low-cost, time-saving, and easy-to-use competitive immunoassay platform to detect SARS-CoV-2 antibodies from clinical saline gargle samples.

2. Materials and methods

2.1. Reagents and samples

Antibody (IgG) to SARS-CoV-2 RBD protein (anti-RBD; Sino Biological US, Inc., Wayne, PA, USA) diluted in 0.9% w/v sterile saline solution was mixed with 1% and 10% w/v pooled human saliva for simulated clinical samples (Innovative Research, Novi, MI, USA). The final concentrations of SARS-CoV-2 antibody in the solutions were varied from 0 to 500 ng/mL. ACE2 (InvivoGene, CA, USA) was used to compare its competitive binding with anti-RBD.

Clinical saline gargle samples from student participants were provided by the University of Arizona, including Ct values obtained from RT-qPCR assays. Details on RT-qPCR can be found in our previous work (Breshears et al., 2022). Heat inactivation was conducted at 65 °C for 30 min. During sample collection, participants were given 5 mL of 0.9% sterile saline solution and completed a 5-s swish followed by a 10-s gargle, all repeated 3 times. The saliva content in the clinical gargle samples was approximately 10%. These samples were additionally diluted 10-fold (the saliva content would be around 1%) with 0.9% w/v sterile saline solution. All experimental protocols and sample collection procedures were approved by the University of Arizona's Institutional Review Board (IRB), number 2102491314.

2.2. Paper microfluidic chips

The chip design was made using SolidWorks 2020 software (Dassault Systèmes, Vélizy-Villacoublay, France). Each chip contained 6 parallel channels composed of 2 circular areas connected to a rectangular channel (Fig. 1c). Specific dimensions can be found in Supplementary Fig. S1. The top circular area was designated for sample loading (loading area), while the next circular area (immediately below) was used for pre-loading antibodies and particle count imaging (test zone). Details of paper microfluidic chip fabrication can be found in the Supplementary Methods.

2.3. Antigen conjugation to fluorescent particles

SARS-CoV-2 RBD antigens (Sino Biological US, Inc.) were covalently conjugated to yellow-green, carboxylated, fluorescent polystyrene particles (diameter = 0.5 μm; Magsphere Inc., Pasadena, CA, USA). Fluorescence of particles was necessary to enable particle counting based on fluorescence microscopic imaging; however, it played no role in flow velocity analysis. Details of antibody conjugation can be found in the Supplementary Methods and in (Liang et al., 2022a, 2022b).

2.4. Competitive particle immunoassay with flow velocity measurement

1 μL of anti-RBD was pre-loaded onto the chip through the test zone (the second circular area) for all 6 channels (Fig. 1c). The anti-RBD solution did not flow beyond the loading area due to the small volume (1 μL), and was kept within the micropores of paper fibers (Ratajczak et al., 2022). It was dried for 3 min to allow antibodies to be mechanically immobilized to the paper substrate. 2 μL of the RBD antigen-conjugated particle suspension (RBD-particles) was also dispensed onto the same test zone in each channel, and the chip was dried completely over 5 min. Again, it did not flow beyond the test zone due to the small volume (2 μL). The chip was then placed in the pre-fabricated chip holder for capturing a video clip with a smartphone camera (Galaxy S10 Lite; Samsung Electronics America, Inc., NJ, USA) (Supplementary Fig. S2a). Samples were loaded from the top loading area, and flowed to the end of the channel due to its larger volume (5 μL), carrying the particles not captured in the test zone via capillary force (Ratajczak and Stobiecka, 2022). Flow velocity profiles were analyzed using our developed Python script on Google Colaboratory running on a cloud. Flow velocities were calculated based on the website app, coded by Dr. Steven Abbott and Dr. Nigel Holmes, available at: https://www.stevenabbott.co.uk/practical-coatings/capillary-flow.php (Supplementary Fig. S3). Details of flow velocity measurements and data analysis can be found in the Supplementary Methods.

2.5. Competitive particle immunoassay with particle counting

After the video was taken for the flow velocity measurement, the chips were allowed to dry fully, taking approximately 10–15 min. Once fully dried, the chips were placed into the imaging setup seen in Supplementary Fig. S2b. Details of this imaging setup can be found in our previous work (Breshears et al., 2022). Each channel in the chip was imaged three times to obtain three different field-of-views (FOVs). Images were processed by ImageJ (US National Institutes of Health; Bethesda, MD, USA) using a custom batch macro shown in Supplementary Code S1. The image was turned into a grayscale image, cropped, and an intensity threshold was applied to minimize background noise. Next, only the particles with 75 pixels or greater were counted to isolate the particles. After images were processed in ImageJ, the average pixel areas from three images were obtained for a single channel. Next, all six channels in a single chip were averaged to replicate the results. These values were then used to create charts. Details can be found in the Supplementary Methods.

2.6. Statistical analysis

For the group comparison between different samples, one-way analysis of variance (ANOVA) tests was performed using GraphPad Prism 9.4.1. Mean values between various concentrations and the control were compared through ANOVA tests, and significant differences were determined. Tukey's honestly significant difference test (Tukey's HSD test) was applied in addition. Welch's *t*-test was used to compare the mean values of virus positive samples and virus negative samples.

3. Results and discussion

3.1. LOD and linear range with simulated clinical saline samples

Initially, IgG antibodies to α strains of SARS-CoV-2 (anti-α-RBD) were spiked to 1% and 10% saliva solutions (both diluted with 0.9% w/v saline). 10% saliva solution is expected to mimic the clinical saline gargle samples, while 1% saliva solution may provide more reproducible results. Antibody concentrations ranged from 0 to 100 ng/mL. RBD antigens from α strains (α-RBD) and ο strain (ο-RBD) were conjugated to the fluorescent particles. The α antibodies should bind to α-RBD-particles, while they should also bind to the ο-RBD-particles to a different extent (cross-reactivity).

Fig. 2a–c shows the results of the particle counting assay. As expected, more particles were found with the negative samples in the test zone (Fig. 2a). With the correct antibody-antigen pair (α antibodies and α-RBD-particles) (Fig. 2b), 1% saliva samples (pink color) showed the expected linear decrease with increasing antibody concentration. The lowest concentration statistically different from the negative control (zero antibodies in 1% saliva) was 5 ng/mL, which is the LOD. The curve was linear from up to 50 ng/mL. However, the 10% saliva samples (blue color) did not show a decreasing linear trend, although its LOD was

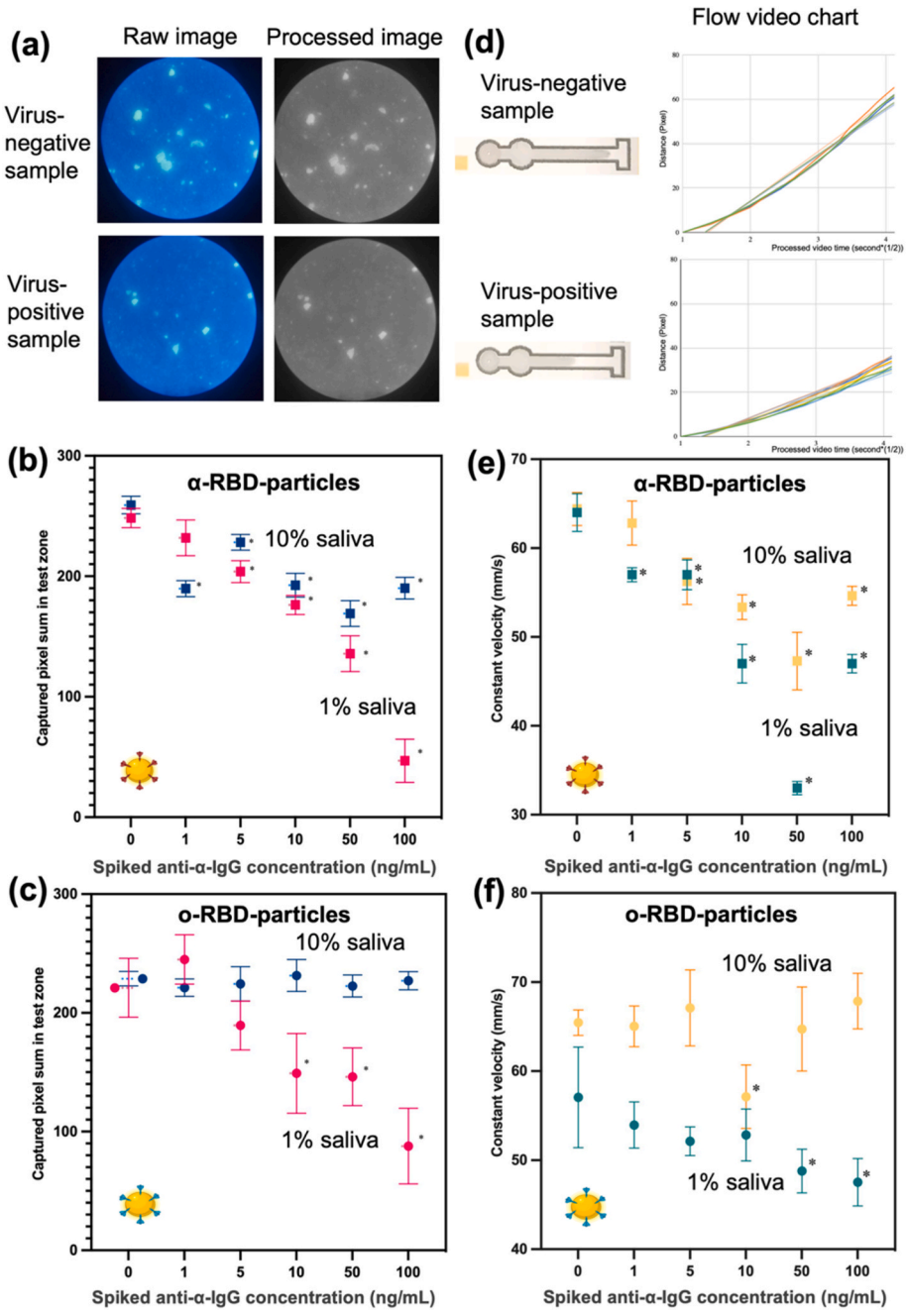

Fig. 2. Assay results with 10% and 1% saliva. Representative raw and processed images of the paper chips are shown in (a). The pixel sums were plotted against the antibody concentration using α-RBD-particles (b) and ο-RBD-particles (c). Representative still images and flow velocity charts from the paper chips are shown in (d). The flow velocities were plotted against the antibody concentration, using α-RBD-particles (e) and ο-RBD-particles (f). All data points are averages and standard deviations from 12 (b and e) or 6 (c and f) independent experiments, each time using different chips. Significant differences ($p < 0.05$) from 0 antibody data are marked *.

better at 1 ng/mL. This trend could be explained by the higher saliva content acting as a stabilizer in the reaction that prevents the antibodies from self-aggregating (thus lower LOD) while capping the extent of antibody-antigen binding (hence saturated signals). Experiments were repeated with incorrect antibody-antigen pair (α antibodies and o-RBD-particles) (Fig. 2c). As expected, the 10% saliva solutions could not detect antibodies. However, with 1% saliva solutions, the linear decreasing trend could be observed (1–100 ng/mL), although the LOD was compromised to 10 ng/mL. Therefore, 10% saliva solutions should be used to minimize the cross-binding of incorrect antibody-antigen pairs and to demonstrate the low LOD of 1 ng/mL 10% dilution also mimics the typical saliva concentrations of clinical saline gargle samples. If quantification is necessary, clinical saline gargle samples (typically at 10%) can be diluted 10-fold at the cost of potential cross-binding.

Fig. 2d–f shows the results of the flow velocity assay. With the correct antibody-antigen pair (α antibodies and α-RBD-particles) (Fig. 2e), 1% saliva samples showed a LOD of 1 ng/mL and a linear range up to 50 ng/mL. Meanwhile, 10% saliva samples showed a LOD of 5 ng/mL and a linear range up to 50 ng/mL. The higher contents of proteins and other molecules in 10% saliva increased the Poiseuille pressure (η) and decreased the capillary pressure (γ and cos θ), interfering with antibody-antigen binding. Thus, the flow velocity assay showed more significant decreases with more diluted (e.g., 1%) saliva solutions. However, there is little difference in choosing between 1% and 10%, as the LOD and linear range of 1% saliva should be multiplied by 10 to compare with those of 10% saliva. With the incorrect antibody-antigen pair (α antibodies and o-RBD-particles) (Fig. 2f), the 10% saliva could not detect antibodies, i.e., minimizing the cross-binding. However, with 1% saliva solutions, there was a weak decreasing trend up to 100 ng/mL, with a much higher LOD of 50 ng/mL. Again, 10% saliva samples should be used to suppress cross-binding (with limited quantitative measurements), while 1% could be used for quantifying antibody concentrations (with limited specificity to variants).

The demonstrated LODs of 1–5 ng/mL in 10% saliva, equivalent to 10–50 ng/mL in undiluted saliva, are substantially lower than or at least comparable to those of other SARS-CoV-2 antibody assays in blood serum or plasma: 57.8 ng/mL using microfluidic particle dam and subsequent microscopic imaging (Wu et al., 2022), 0.08 ng/mL in diluted plasma = 80 ng/mL in undiluted plasma using gold nanospikes and localized surface plasmon resonance (LSPR) in an optomicrofluidic chip (Funari et al., 2020). Commercial enzyme-linked immunosorbent assay (ELISA) showed the LOD of 13,500 ng/mL in serum or plasma (Funari et al., 2020).

To establish calibration curves, we conducted additional experiments using α-RBD particles with the anti-α-IgG concentrations ranging from 0 to 50 ng/mL, i.e., 0, 5, 10, 15, 20, 25, 30, 35, 40, 45, and 50 ng/mL, in 10% and 1% saliva solutions (Fig. 3). The particle counting assay showed a narrower linear range from 20 to 50 ng/mL with R^2 values of 0.815 and 0.844. The flow velocity assay showed a broader linear range from 0 to 50 ng/mL, while R^2 was good (0.856) only at 1% saliva. Previous studies tested the half maximal inhibitory concentration (IC_{50}) of the antibody was from 7 to 1476 ng/mL to neutralize alpha RBD (50 mg/mL) (Windsor et al., 2022). This range is within our linear detection range. The regression equations could also potentially be used as a reference to quantify salivary antibody content.

3.2. Comparison between ACE2 and Anti-RBD

The RBD antigen of SARS-CoV-2 binds to its human receptor ACE2 to mediate the virus from entering the cell. The high binding affinity of ACE2 to RBD was reported in recent studies and is potentially related to the virus's immune evasion, cell infectivity, and widespread (Fig. 4a) (Shang et al., 2020). To demonstrate the competitive interactions between ACE2 and anti-RBD with α-RBD and o-RBD, we added 1 ng/mL ACE2 to the testing samples (10% saliva) and repeated two assays (Fig. 4b). As expected, both assays' signal changes (particle counting and flow velocities) were significantly smaller than those without ACE2 since the antibody-antigen binding was blocked by ACE2 (Fig. 4c,f). In addition, they did not show any linearly decreasing trends (Supplementary Fig. S6). When comparing the signals at zero antibody concentrations, those with ACE2 were smaller, 130–170 with particle counting and 44–59 with flow velocity (Fig. 4d,g), than those without ACE2 – 230 with particle counting and 65 with flow velocity (Fig. 2b,c,e,f). Such smaller signals indicate a strong binding between ACE2 and RBD protein, allowing particles to leave the test zone and reduce the interfacial tension at the moving front.

We repeated both particle counting and flow velocity assays for 1 ng/mL anti-α-RBD or 1 ng/mL ACE2 (assayed separately), both in 10% saliva, using either α-RBD-particles or o-RBD-particles. With particle counting, no statistical difference could be found ($p > 0.05$) between anti-α-RBD and ACE2 with α-RBD-particles (Fig. 4e). This result is expected since both anti-α-RBD and ACE2 can correctly bind to α-RBD-particles. However, a significant difference could be found ($p < 0.0001$) with o-RBD-particles (Fig. 4e). Again, this is expected since anti-α-RBD cannot perfectly bind to o-RBD-particles, while ACE2 can still bind to o-

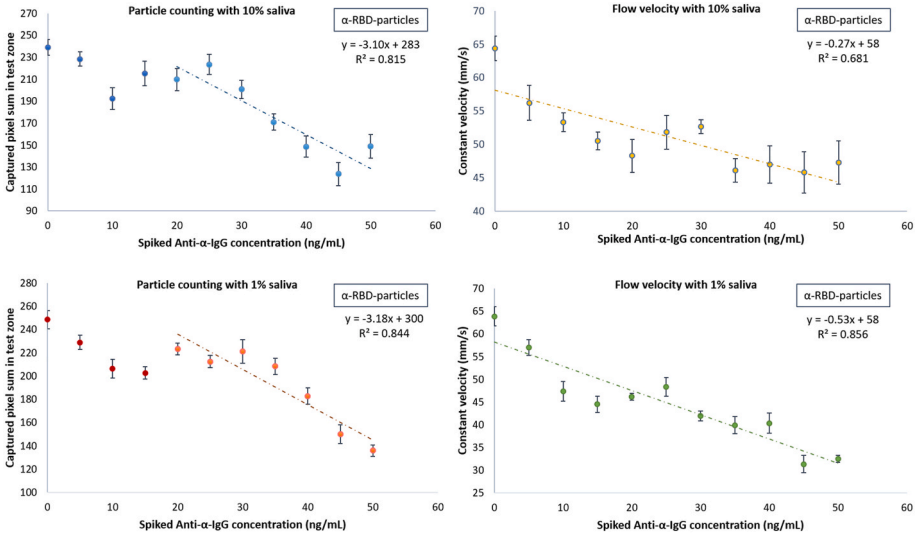

Fig. 3. Linear regressions with 10% and 1% saliva using α-RBD particles. Particle counting and flow velocity were measured against antibody concentration. All data points are averages and standard deviations from 12 independent experiments, each time using different chips.

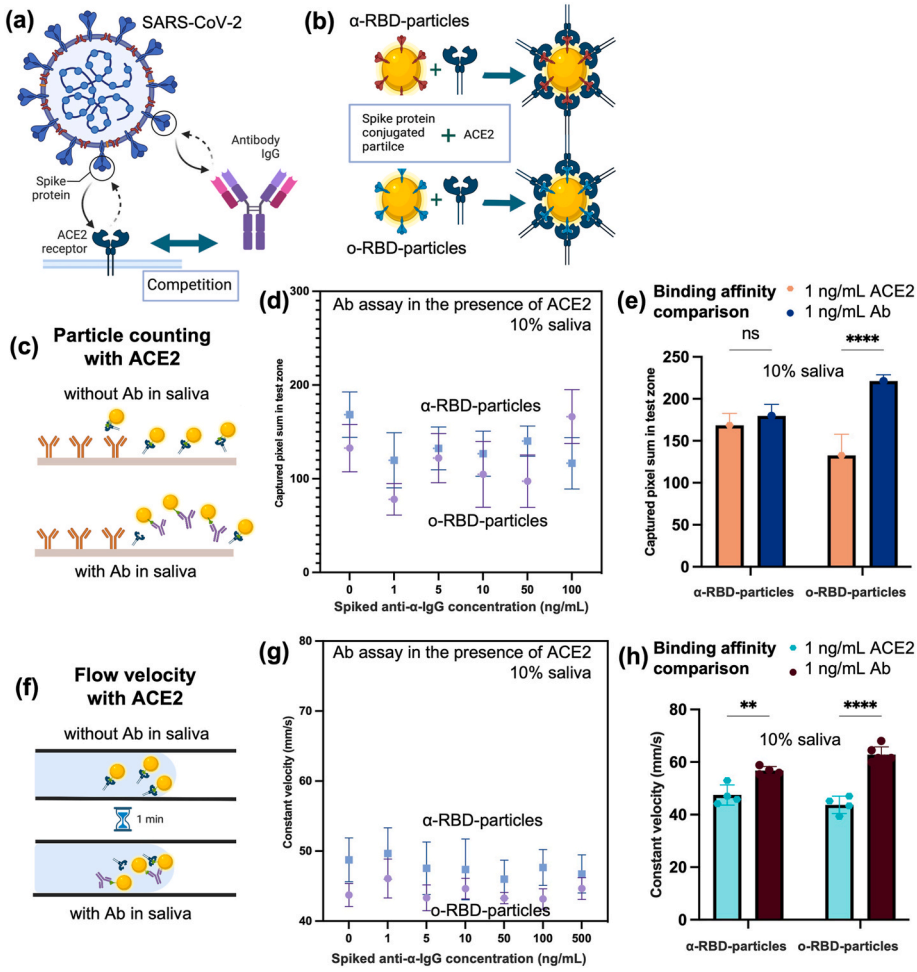

Fig. 4. Competition between ACE2 and antibody. Schematic illustration (a) is shown for spike protein to compete with ACE2 receptor and IgG antibody (anti-RBD). Both α-RBD-particles and o-RBD-particles can bind to ACE2 (b). Particle counting (c) and flow velocity assays (f) were conducted for assaying IgG antibodies in the presence of 1 ng/mL ACE2 in 10% saliva (d,g), and for separately assaying 1 ng/mL ACE2 and 1 ng/mL IgG antibody in 10% saliva (e,h). All data points are averages and standard deviations from 6 independent experiments, each time using different chips. Significant differences from 0 antibody data are marked ** ($p < 0.01$) and **** ($p < 0.0001$).

RBD-particles. Interestingly, the signal decrease was more significant with ACE2 and o-RBD-particles, potentially implying the wider spread of omicron strains. With flow velocity, statistical differences could be found not only between anti-α-RBD and ACE2 with α-RBD-particles ($p < 0.01$) but also between anti-α-RBD and ACE2 with o-RBD-particles ($p < 0.0001$) (Fig. 4h). This result potentially indicates the stronger binding affinity of ACE2 to RBD than anti-RBD to RBD, especially when assayed with flow velocities. Such stronger affinity may contribute to highly efficient cell entry while evading immune surveillance (Shang et al., 2020).

3.3. Clinical samples

Clinical saline gargle samples were collected at the beginning of the α variant outbreak. Saliva contents were around 10%. Samples were competitively assayed using α-RBD-particles, and first assayed with the particle counting assay. While the average pixel sums were higher for the virus-negative samples than the virus-positive ones, there was little difference between two groups as shown in Fig. 5b. Specifically, the pixel sums of the virus-positive samples varied significantly, potentially because not all virus-positive samples were antibody-positive (while all virus-negative samples should be antibody-negative). Alternatively, the antibody concentration could be too high (outside the linear range), contributing to the false-negative results. To confirm the latter, we prepared a separate set of virus-negative and virus-positive samples, each diluted 10-fold (saliva contents became approximately 1%). A statistical significance existed ($p < 0.01$) between virus-negative and virus-positive samples, despite the assays targeting antibodies, not virus antigens (Fig. 5c). A clear separation can be made between negatives and positives at the pixel sum of 260. This result indicates the need for a dilution when the antibody level is too high. One virus-positive clinical sample was antibody-negative, i.e., samples were collected too early before antibody development.(Hartanto et al., 2020). The immune seroconversion reaches its maximum typically after 5–7 days of symptom onset for IgG and several days later for IgM.

Long et al. demonstrated that IgG antibody production reaches its maximum after 5–7 days and IgG's are present in 90% of patients 14 days from the onset of the SARS-CoV-2 symptoms (Long et al., 2020). Since the current IRB protocol did not allow us to collect any information when the symptom started (to maintain the confidentiality of the subjects' medical information), we could not do further analyses in distinguishing antibody-positive and antibody-negative samples. Nonetheless, we do not believe that most subjects waited over 7 days. Since our assay is sufficiently sensitive to detect the small number of neutralizing antibodies, as demonstrated in the previous sections, we might have detected the small number of neutralizing antibodies during their initial immune responses. Details of each individual's testing results via particle counting are shown in Supplementary Fig. S4.

Flow velocity assay was also applied to the clinical samples. Without dilution, there was little difference between virus-negative and virus-positive samples (as determined by RT-qPCR), as shown in Fig. 6b. 10-fold dilutions were made, and the results showed a statistical difference ($p < 0.001$) between negatives and positives (Fig. 6c). A clear separation can be made at the flow velocity of 60 mm/s. Again, one virus-positive clinical sample was antibody-negative, which was identical to the particle counting results. Details of each individual's testing

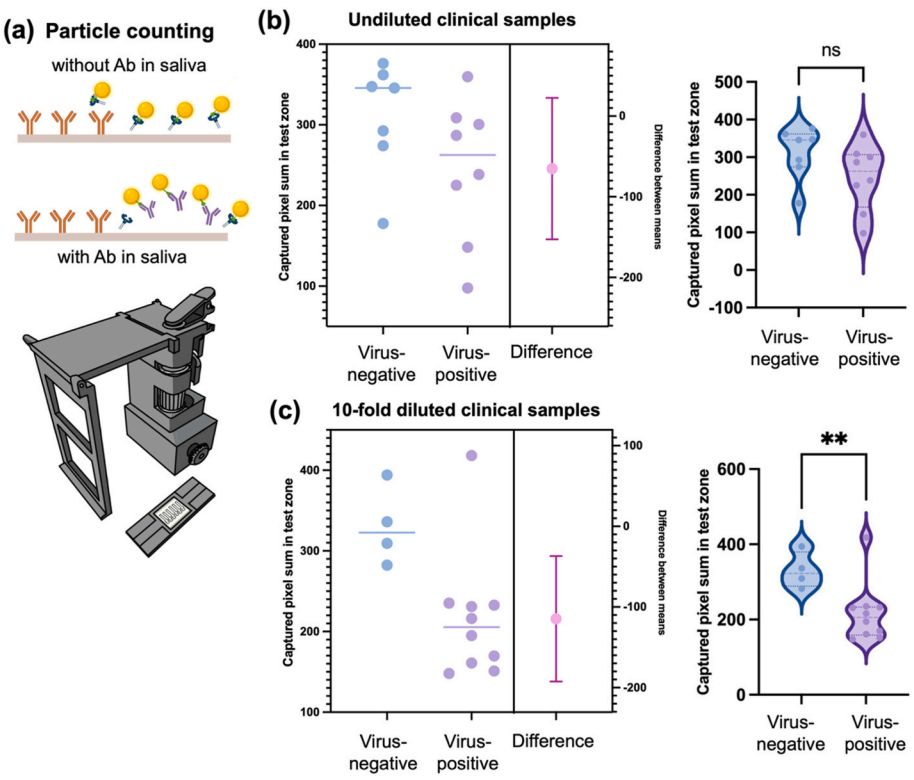

Fig. 5. Particle counting assays with clinical samples. Particle counting (a) and α-RBD-particles were used. The results with virus-negative and virus-positive (as confirmed by RT-qPCR) were grouped together and the mean difference between two groups are also shown. Undiluted (b) and 10-fold diluted (c) clinical samples were assayed. All data points are averages from 6 independent experiments, each time using different chips. Standard deviations were not shown for clarity. Significant differences from 0 antibody data are marked ** ($p < 0.01$).

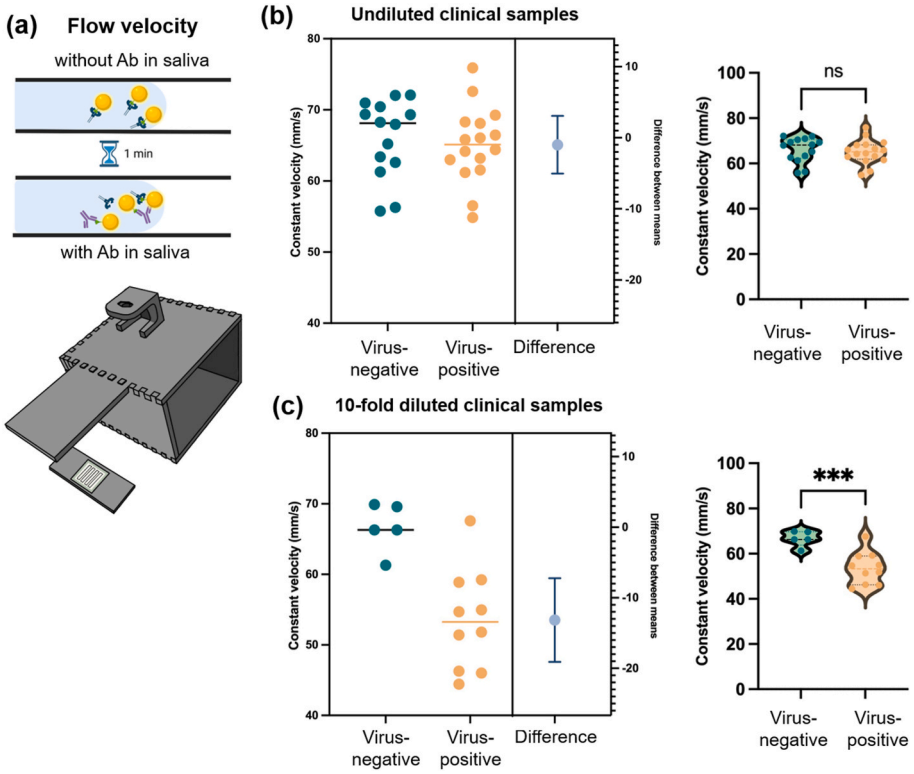

Fig. 6. Flow velocity assays with clinical samples. Flow velocity measurements (a) and α-RBD-particles were used. The results with virus-negative and virus-positive (as confirmed by RT-qPCR) were grouped together and the mean difference between two groups are also shown. Undiluted (b) and 10-fold diluted (c) clinical samples were assayed. All data points are averages from 6 independent experiments, each time using different chips. Standard deviations were not shown for clarity. Significant differences from 0 antibody data are marked *** ($p < 0.001$).

results via flow velocity are shown in Supplementary Fig. S5.

3.4. Comparison of two methods

Two different detection methods – particle counting and flow velocity – were used to analyze the competitive particle immunoassay of SARS-CoV-2 IgG salivary antibodies on paper microfluidic chips. Supplementary Fig. S7 summarizes the time scale of these two methods. Flow velocity assay required 12 min from sample-to-answer, or 2 min if the antibodies and antigen-particles were pre-loaded prior to the assays.

On the other hand, particle counting assay required 27–32 min from sample-to-answer, or 17–22 min if the pre-loading was prepared before the assay. The flow velocity method was faster in assay time than the particle counting since the solution did not need to be incubated for an additional 10–15 min after the flow reached the other end. Additionally, the particle counting method required additional 5 min for image capture since three images should be taken from each channel. However, the data analysis time was faster with particle counting since it utilized a batch macro code running on ImageJ. On the other hand, the flow velocity method required a specialized code running on Google Colab that was more time-consuming. Considering this assay time and the device's simplicity, flow velocity measurement is a winner for SARS-CoV-2 IgG salivary antibody assay.

LODs were comparable between 10% and 1% saliva solutions for both particle counting and flow velocity methods. However, assay linearities were improved with 1% saliva compared to 10%. The clinical saline gargle experiments also showed better distinction with 10-fold dilutions (roughly equivalent to 1% saliva). On the other hand, the cross-binding to omicron strains was minimized with 10% saliva compared to 1%. Therefore, we can conclude that 1% saliva (or 10-fold diluted saline gargle sample) should be used to quantify antibodies, and 10% saliva (or undiluted saline gargle sample) should be used as a complementary tool for variant identification.

Overall, we presented low-cost, rapid, smartphone-based salivary IgG detection platforms. The portability and simplicity of this platform could meet the requirements for public or household detection towards a low-cost public health monitoring tool.

CRediT authorship contribution statement

Yan Liang: Conceptualization, Data curation, Formal analysis, Investigation, Methodology, Software, Validation, Visualization, Writing – original draft. **Bailey C. Buchanan:** Conceptualization, Data curation, Formal analysis, Investigation, Methodology, Software, Validation, Writing – original draft. **Bradley Khanthaphixay:** Data curation, Investigation, Methodology. **Avory Zhou:** Data curation, Investigation, Methodology. **Grace Quirk:** Resources. **Michael Worobey:** Funding acquisition, Project administration, Resources, Supervision, Project administration. **Jeong-Yeol Yoon:** Conceptualization, Formal analysis, Funding acquisition, Methodology, Project administration, Supervision, Visualization, Writing – review & editing.

Declaration of competing interest

The authors declare that they have no known competing financial interests or personal relationships that could have appeared to influence the work reported in this paper.

Data availability

Data will be made available on request.

Acknowledgments

This work was supported by the Technology and Research Initiative Fund (TRIF) of the Arizona Board of Regents (ABOR) and the Provost Investment Fund (PIF) of the University of Arizona. It was also supported by the University of Arizona Biological Chemistry Program Fellowship associated with the US National Institutes of Health – National Institute of General Medical Sciences (NIH-NIGMS), grant number T32 GM08804.

Appendix A. Supplementary data

Supplementary data to this article can be found online at https://doi.org/10.1016/j.bios.2023.115221.

References

Akarapipad, P., Kaarj, K., Breshears, L.E., Sosnowski, K., Baker, J., Nguyen, B.T., Eades, C., Uhrlaub, J.L., Quirk, G., Nikolich-Žugich, J., Worobey, M., Yoon, J.-Y., 2022. Biosens. Bioelectron. 207, 114192 https://doi.org/10.1016/j.bios.2022.114192.

Alkharaan, H., et al., 2021. J. Infect. Dis. 224, 407–414. https://doi.org/10.1093/infdis/jiab256.

Breshears, L.E., Nguyen, B.T., Akarapipad, P., Sosnowski, K., Kaarj, K., Quirk, G., Uhrlaub, J.L., Nikolich-Žugich, J., Worobey, M., Yoon, J.-Y., 2022. PNAS Nexus 1, pgac028. https://doi.org/10.1093/pnasnexus/pgac028.

Cubas-Atienzar, A.I., Kontogianni, K., Edwards, T., Wooding, D., Buist, K., Thompson, C. R., Williams, C.T., Patterson, E.I., Hughes, G.L., Baldwin, L., Escadafal, C., Sacks, J. A., Adams, E.R., 2021. Sci. Rep. 11, 18313 https://doi.org/10.1038/s41598-021-97489-9.

Funari, R., Chu, K.-Y., Shen, A.Q., 2020. Biosens. Bioelectron. 169, 112578 https://doi.org/10.1016/j.bios.2020.112578.

Hartanto, H., Wu, M., Lam, M.L., Chen, T.-H., 2020. Biomicrofluidics 14, 061507. https://doi.org/10.1063/5.0031521.

Heinz, F.X., Stiasny, K., 2021. npj Vaccines 6, 1–13. https://doi.org/10.1038/s41541-021-00369-6.

Huang, Y., Yang, C., Xu, X., Xu, W., Liu, S., 2020. Acta Pharmacol. Sin. 41, 1141–1149. https://doi.org/10.1038/s41401-020-0485-4.

Kalish, H., et al., 2021. Sci. Transl. Med. 13, eabh3826 https://doi.org/10.1126/scitranslmed.abh3826.

Khoury, D.S., Cromer, D., Reynaldi, A., Schlub, T.E., Wheatley, A.K., Juno, J.A., Subbarao, K., Kent, S.J., Triccas, J.A., Davenport, M.P., 2021. Nat. Med. 27, 1205–1211. https://doi.org/10.1038/s41591-021-01377-8.

Klug, K.E., Reynolds, K.A., Yoon, J., 2018. Chem. Eur J. 24, 6025–6029. https://doi.org/10.1002/chem.201800085.

Kopel, J., Goyal, H., Perisetti, A., 2021. 34, 63–72. https://doi.org/10.1080/08998280.2020.1829261.

Liang, Y., Zhou, A., Bever, C.S., Cheng, L.W., Yoon, J.-Y., 2022a. Microchim. Acta 189, 322. https://doi.org/10.1007/s00604-022-05407-1.

Liang, Y., Zhou, A., Yoon, J.-Y., 2022b. ACS Omega 7, 30064–30073. https://doi.org/10.1021/acsomega.2c03099.

Long, Q.-X., et al., 2020. Nat. Med. 26, 845–848. https://doi.org/10.1038/s41591-020-0897-1.

Norman, M., et al., 2020. Nat. Biomed. Eng. 4, 1180–1187. https://doi.org/10.1038/s41551-020-00611-x.

Rai, P., Kumar, B.K., Deekshit, V.K., Karunasagar, I., Karunasagar, I., 2021. Appl. Microbiol. Biotechnol. 105, 441–455. https://doi.org/10.1007/s00253-020-11061-5.

Ratajczak, K., Sklodowska-Jaros, K., Kalwarczyk, E., Michalski, J.A., Jakiela, S., Stobiecka, M., 2022. Int. J. Mol. Sci. 23, 8694. https://doi.org/10.3390/ijms23158694.

Ratajczak, K., Stobiecka, M., 2022. Carbohydr. Polym. 229, 115463 https://doi.org/10.1016/j.carbpol.2019.115463.

Shang, J., Wan, Y., Luo, C., Ye, G., Geng, Q., Auerbach, A., Li, F., 2020. Proc. Natl. Acad. Sci. U.S.A. 117, 11727–11734. https://doi.org/10.1073/pnas.2003138117.

To, K.K.-W., et al., 2020. Lancet Infect. Dis. 20, 565–574 https://doi.org/10.1016/S1473-3099(20)30196-1.

Tollånes, M.C., Kran, A.-M.B., Abildsnes, E., Jenum, P.A., Breivik, A.C., Sandberg, S., 2020. Clin. Chem. Lab. Med. 58, 1595–1600. https://doi.org/10.1515/cclm-2020-0628.

Windsor, I.W., Tong, P., Lavidor, O., Moghaddam, A.S., McKay, L.G.A., Gautam, A., Chen, Y., MacDonald, E.A., Yoo, D.K., Griffths, A., Wesemann, D.R., Harrison, S.C., 2022. Sci. Immunol. 7, eabo3425 https://doi.org/10.1126/sciimmunol.abo3425.

Wu, M., Wu, S., Wang, G., Liu, W., Chu, L.T., Jiang, T., Kwong, H.K., Chow, H.L., Li, I.W. S., Chen, T.-H., 2022. Sci. Adv. 8, eabn6064 https://doi.org/10.1126/sciadv.abn6064.

Yakoh, A., Pimpitak, U., Rengpipat, S., Hirankarn, N., Chailapakul, O., Chaiyo, S., 2021. Biosens. Bioelectron. 176, 112912 https://doi.org/10.1016/j.bios.2020.112912.

Younes, N., Al-Sadeq, D.W., AL-Jighefee, H., Younes, S., Al-Jamal, O., Daas, H.I., Yassine, H.M., Nasrallah, G.K., 2020. Viruses 12, 582. https://doi.org/10.3390/v12060582.